JOURNAL

of the AMERICAN CERAMIC SOCIETY

Volume 67, No. 3 March 1984

Fracture of Ceramic-Polymer Composite Biomaterials

S. YALVAÇ* and J. H. HAND†

Department of Chemical Engineering, The University of Michigan, Ann Arbor, Michigan 48109

Fracture toughness, strength, and elastic modulus of poly(methyl methacrylate) (PMMA)- and poly(butyl methacrylate) (PBMA)-impregnated alumina ceramics were measured as a function of polymer volume fraction, mean polymer particle size, and interfacial bonding between the polymer and ceramic. Fracture toughness was found to increase with increasing polymer volume fraction and decreasing polymer particle size. Interfacial bonding played a very important role in determining the fracture mode, which was interparticle and intraparticle when the interface was coupled and uncoupled, respectively. Poly(methyl methacrylate) increased the fracture toughness of the ceramic 1.5 to 2 times more effectively than poly(butyl methacrylate). The elastic modulus was found to be unaffected by impregnation. The previously reported Bowie model was modified and proved to be useful. Single- and double-crack versions of this model predicted strengths somewhat higher than those measured. This discrepancy and the scatter in the data were explained by the crack-path tortuousity and the possibility of different mechanisms operating in different samples. Fractographs of the selected bend specimens were taken to support this argument.

I. Introduction

THE search for surgical materials suitable for permanent joint replacement has lead biomaterials researchers to porous materials. When implanted in bone, porous materials allow bony ingrowth, potentially aiding in fixation of devices such as hips, knees, and shoulder replacements. Pore structures best for bone-tissue ingrowth must contain highly interconnected porosity with pore interconnection sizes of ≥ 100 μm.[1,2]

Several porous biomaterials have been reported in the literature. They include poly(vinyl chloride) sponge,[3] acrylamide sponge,[4] ceramic-epoxy composite,[5] and titanium.[6] Clinical studies of these composites in laboratory animals showed the formation of a strong bond between the bone and implant due to bone growth into the pores.

Composites based on polymer impregnation of porous materials have been attracting much attention in engineering and bioengineering circles. Most matrices have included ceramic tile,[7] cement and concrete,[8-11] ceramic,[12] and wood.[13-16] Strength increases by a factor of four and two-fold increases in moduli of elasticity and large improvements in corrosion resistance and durability have been reported for polymer-impregnated concrete as compared to unfilled concrete. Two- to three-fold increases in flexural, compressive, and tensile strengths, and impact resistance were obtained for polymer-impregnated ceramic tile bodies. Similar improvements were reported for polymer-wood composites.

This study investigates the properties of ceramic-polymer composites which have the advantages of the ceramic phase without the unpredictable strength and characteristic brittleness of such materials. The incorporated polymer phase is designed to reduce the brittleness of the host material, improving its energy-absorbing properties during crack initiation and propagation, while retaining the other excellent chemical, mechanical, and biological properties of ceramics. Careful removal of polymer from a thin surface layer of the composite will leave a porous region for bone-tissue ingrowth.

II. Material Preparation and Testing

The procedure followed for the fabrication of the porous ceramic matrix was similar to that of Klawitter *et al.*[17] The starting material was a reactive fine-grained alumina powder.‡ A viscous slip was prepared by admixing 540 mL of 4 wt% aqueous solution of poly (vinyl alcohol)§ as a binding agent with 1200 g of alumina. About 0.05% (dry weight basis) citric acid with 0.1% (dwb) Darvan No. 7¶ was also added as a deflocculant. A foaming agent (30% hydrogen peroxide) was then added to the slip and thoroughly mixed. Eight drops of whole citrated blood were added as a catalyst to decompose the peroxide. The catalyst was mixed into the slip and, within 30 s, the slip was infiltrated into a high-porosity polyurethane sponge,** where the peroxide decomposed to form a foam. The sponge used was a reticulated, fully open pore, flexible ester-type of polyurethane foam. It is characterized by a three-dimensional skeletal structure of strands which provide a constant 97% void space and a very high degree of permeability. The pore size of the sponge material is characterized by the number of pores per linear centimeter (ppc) and is available over a range of 4 to 40 ppc.

After the foaming operation, the material was allowed to dry at room temperature for a week and then dried in an oven at 125°C for 24 h. The high-alumina foamed material was then sintered in air at 1500°C for 18 h and cooled slowly to room temperature. The polyurethane sponge burned away during firing, leaving free, interconnected spaces in the resulting body.

Received August 19, 1982; revised copy received November 14, 1983; approved January 3, 1984.

Supported by the National Institute of Health under Grant No. GM22447.

*Now with Dow Chemical USA, Midland, Michigan 48640.

†Now with Dow Corning Corporation, Midland, Michigan 48640.

‡A-17 reactive alumina, Aluminum Company of America, Pittsburgh, PA.

§Vinol 205, Air Products and Chemicals, Allentown, PA.

¶R. T. Vanderbilt Co., Inc., Norwalk, CT.

**Scott Paper Co., Chester, PA.

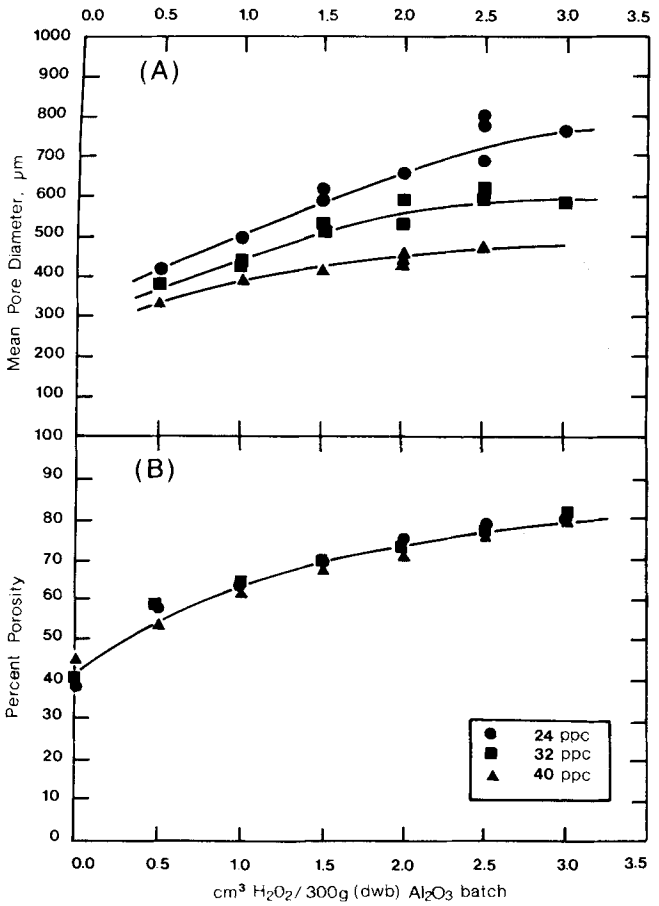

Fig. 1. (*A*) Pore size and (*B*) porosity calibration curves for polyurethane sponges with pore sizes indicated as a function of foaming agent concentration.

It was found that percent porosity and the average pore size of the final ceramic depended both on the amount of foaming agent and the ppc size of the sponge used, as shown in Fig. 1. This result differs from that of Klawitter *et al.*[17] They claimed to have achieved control over the mean pore size by varying the amount of foaming agent. In this work, it was found that the pore size of the matrix is governed both by the ppc size of the sponge and the concentration of the foaming agent. As expected, the porosity was found to increase with increasing amount of foaming agent and decreasing ppc size of the sponge. It was possible to hold either the porosity or average pore size constant and vary the other parameter by choosing the correct amount of foaming agent and sponge size.

The porosity of the fired ceramic matrix was determined from true and apparent density measurements. The true density of alumina, d_t, was determined in accordance with ASTM C135–66[18] using a standard pycnometric method; it was found to be 3.91 g/cm^3. The apparent density, d_a, was calculated from measurements of ceramic matrix dimensions and weight. The percent porosity was then calculated using the equation

$$P = (d_t - d_a)/d_t \times 100 \quad (1)$$

The average lineal pore size, D, was calculated from optical micrographs of the specimen using techniques described by Kingery[19] and Hulbert *et al.*[20]

To form bonded composites, ceramic matrices which had the desirable combination of porosity and pore size were first evacuated to a pressure of 0.67 Pa for ≈ 30 min and then treated with 0.2% aqueous solution of technical-grade silane coupling agent (γ-methacryloxypropyltrimethoxysilane),[††] followed by drying at 95°C for 24 h. The control samples tested for studying the effect of bonding the interface were not treated with the silane coupling agent.

To form the composites, ceramic matrices were evacuated, immersed in liquid monomer-initiator solution, and brought back to atmospheric pressure. The initiator employed was 0.1% by weight of 2,2′-azobis [2-methylpropionitrile]. Monomers chosen were selected to yield polymers displaying different dynamic behavior at body temperature; methylmethacrylate and butylmethacrylate yielded a glossy and rubbery polymer, respectively. Polymerization was accomplished by slowly raising the temperature from 30° to 70°C over seven days. This slow polymerization was necessary to avoid void spaces in the polymer due to boiling monomer.

Filling of the pore spaces was determined from density measurements and qualitatively studied by scanning electron microscopy (SEM). Filling of the pore space varied from 90 to 100%. For most samples, filling was more than 94%.

Polymer-impregnated ceramics were cut into 0.114 by 0.025 by 0.013 m test specimens and surfaces were machined parallel. All measurements were taken at room temperature under three-point loading conditions in a Ringer's lactate solution to simulate a physiological environment. Prior to testing, all specimens were equilibrated in solution for two weeks. Earlier studies[21–24] indicated that a two-week soaking period is sufficient to bring the polymer to equilibrium. No attempt, however, was made in this investigation to determine the effect of Ringer's lactate on mechanical properties of the composite.

Two steel knife edges to support a crack opening displacement gage (COD gage) were mounted on each fracture-toughness test specimen using a cyanoacrylate adhesive. The COD gage was designed and fabricated according to the available literature[25] and tested and calibrated using a COD gage calibration fixture.[‡‡]

Two commonly used, but fundamentally different methods of measuring fracture toughness or critical strain energy release rate were used to determine whether the experimental method would affect the results. In the compliance calibration technique (CCT),[26–28] the work done to produce a unit area of fracture surface is measured directly. The second procedure, the ASTM method,[29] determines the surface energy indirectly, but the stress intensity factor directly. Since both methods require a notched bar of the same geometry and similar test procedures, two data points, one for each method, can be measured using only one test specimen. This allowed for efficient use of the test material, which is rather time-consuming to prepare.

Both methods require that fracture-toughness parameters be obtained using precracked specimens. These precracks are usually created by fatigue or thermal shock of the test material. Presence of the ceramic phase made it difficult to fatigue-crack the samples in a controllable fashion. Presence of the polymer phase, on the other hand, did not allow the thermal shock method to be applied to the material, as is common with ceramics. Therefore, a 0.15-mm-wide notch simulating the natural crack was machined in all test specimens.

For a linear elastic material, CCT measures the critical strain energy release rate, G_c, directly from the following equation

$$G_c = (P^2_{max}/2bw)\,[\partial S/\partial(a/w)] \quad (2)$$

where S is the compliance and $\partial S/\partial(a/w)$ is the slope of the S vs a/w curve evaluated for the crack length, a, at the onset of crack instability. Here b and w are the specimen width and depth, respectively, and P_{max} is the load at which the instability occurs.

To obtain the compliance vs a/w data, midspan specimen deflections, Δ, were measured with an extensometer.[§§] An exponential polynomial regression fit to the experimental data points was obtained in order to express the specimen compliance as a function of a/w. These compliance equations can be differentiated easily with respect to a/w and they are reported elsewhere.[30]

The ASTM method measures the critical stress intensity factor, K_{Ic}, directly. The expression used for a simple-edge-notched speci-

[††]Designation Z-6030, Dow Corning Corp., Midland, MI.

[‡‡]Instron Corp., Canton, MA.
[§§]Instron Corp.

Table I. K_{Ic} and G_c Data for Coupled and PMMA-Impregnated Alumina Ceramic

Composite*	G_c (J/m²)†	K_{Ic} (MPa·m$^{1/2}$) CCT method	K_{Ic} (MPa·m$^{1/2}$) ASTM method	$(a/w)f$‡
45.45C-PMMA506	161.8	3.43	2.65	0.47
45.45C-PMMA506	161.7	3.43	3.03	0.48
49.97C-PMMA504	177.8	3.29	3.15	0.47
49.97C-PMMA504	182.9	3.34	2.56	0.49
51.47C-PMMA504	148.8	2.92	3.63	0.43
51.47C-PMMA504	169.2	3.12	3.53	0.50
52.57C-PMMA540	254.4	3.74	2.81	0.49
52.57C-PMMA540	169.2	3.05	2.38	0.47
55.46C-PMMA484	217.0	3.27	2.54	0.50
55.83C-PMMA536	215.3	3.23	2.81	0.48
55.83C-PMMA536	193.0	3.05	2.69	0.59
56.25C-PMMA606	160.3	2.76	2.39	0.56
56.25C-PMMA606	202.2	3.10	2.89	0.51
57.26C-PMMA417	319.4	3.81	2.55	0.46
57.26C-PMMA417	267.7	3.50	2.43	0.49
57.48C-PMMA659	203.5	3.04	2.37	0.54
58.01C-PMMA605	183.4	2.85	1.95	0.52
58.49C-PMMA509	290.9	3.56	3.91	0.53
58.49C-PMMA509	169.1	2.71	2.59	0.48
58.49C-PMMA509	201.7	2.96	2.81	0.48
60.62C-PMMA498	349.8	3.74	3.17	0.53
60.62C-PMMA498	347.5	3.73	3.12	0.56
60.62C-PMMA498	367.6	3.83	3.37	0.51
62.33C-PMMA673	337.4	3.55	2.21	0.57
62.33C-PMMA673	273.9	3.20	2.16	0.50
62.45C-PMMA618	265.4	3.14	1.80	0.48
62.45C-PMMA618	262.3	3.12	1.87	0.49
63.01C-PMMA452	286.1	3.23	3.37	0.46
63.01C-PMMA452	263.2	3.09	3.03	0.51
64.13C-PMMA491	243.2	2.91	3.18	0.51
64.13C-PMMA491	233.2	2.85	2.66	0.48
64.13C-PMMA491	217.3	2.75	2.73	0.46
64.39C-PMMA387	474.8	4.04	3.58	0.46
64.39C-PMMA387	508.7	4.19	3.56	0.48
65.07C-PMMA400	311.1	3.23	1.95	0.53
65.42C-PMMA405	312.2	3.21	2.39	0.51
64.42C-PMMA405	449.6	3.86	2.92	0.47
65.42C-PMMA405	591.7	4.42	3.97	0.58
65.70C-PMMA600	385.0	3.55	2.30	0.59
65.70C-PMMA600	379.6	3.52	2.12	0.51
67.40C-PMMA481	429.2	3.62	2.97	0.49
67.40C-PMMA481	366.3	3.35	2.67	0.60

*In composite sample designations, e.g. 45.45C-PMMA506, the first number indicates volume percent polymer; C and U indicate whether the interface is coupled or uncoupled, respectively; the abbreviation for the type of polymer used to impregnate the ceramic matrix follows the hyphen; and the last number represents the average polymer particle size (or average pore size in the ceramic matrix) in micrometers. †Calculated from Eq. (2). ‡(a/w) value at fracture.

men in three-point bending is given by

$$K_Q = (P_Q S/bw^{3/2})[2.9(a/w)^{1/2} - 4.6(a/w)^{3/2} + 21.8(a/w)^{5/2} - 37.6(a/w)^{7/2} + 38.7(a/w)^{9/2}] \quad (3)$$

where P_Q is the conditional load at fracture as described in the ASTM method,[29] S is the span, and a, b, and w have their previous meanings.

In plane-strain conditions, the fracture-toughness parameters K_{Ic} and G_c are related by

$$K_{Ic} = [EG_c/(1 - \nu^2)]^{1/2} \quad (4)$$

where ν is the Poisson ratio. The value of the term $(1 - \nu^2)^{1/2}$ is usually assumed to be 1. Any error resulting from this practice will be small (<5%) and conservative.

The surfaces of the modulus test specimens were wiped clean with isopropanol-dampened cleaning tissue. A 350-Ω strain gage[¶¶] was mounted on the tension surface, electrical leads were soldered in place, and the assembly was coated with one layer of paraffin wax and one layer of nitrile rubber to stabilize the gage in the hostile Ringer's lactate environment. The rubber was allowed to cure overnight. A second layer of nitrile rubber was applied in the morning and allowed to cure.

[¶¶]Micro-Measurements Div., Vishay Intertechnology, Inc., Romulus, MI.

Table II. K_{Ic} and G_c Data for Uncoupled and PMMA-Impregnated Alumina Ceramic

Composite	G_c (J/m²)*	K_{Ic} (MPa·m$^{1/2}$) CCT method	K_{Ic} (MPa·m$^{1/2}$) ASTM method	$(a/w)f$
52.65U-PMMA521	42.1	1.52	0.84	0.56
52.65U-PMMA521	41.4	1.51	1.07	0.51
52.65U-PMMA521	41.6	1.51	1.17	0.56
60.90U-PMMA447	52.9	1.45	1.11	0.47
60.90U-PMMA447	56.0	1.49	0.96	0.59
60.90U-PMMA447	62.6	1.57	1.05	0.52

*Calculated from Eq. (2).

Table III. K_{Ic} and G_c Data for Coupled and PBMA-Impregnated Alumina Ceramic

Composite	G_c (J/m²)*	K_{Ic} (MPa·m$^{1/2}$) CCT method	K_{Ic} (MPa·m$^{1/2}$) ASTM method	$(a/w)f$
45.32C-PBMA547	122.9	3.00	2.25	0.49
45.32C-PBMA547	146.9	3.28	1.75	0.47
45.32C-PBMA547	171.6	3.55	2.51	0.59
46.90C-PBMA516	150.7	3.22	1.89	0.48
46.90C-PBMA516	151.9	3.23	1.91	0.60
62.31C-PBMA465	254.2	3.08	1.12	0.46
65.87C-PBMA383	279.5	3.01	1.30	0.59
65.87C-PBMA383	248.5	2.84	1.04	0.45
65.87C-PBMA383	276.5	3.00	1.29	0.49

*Calculated from Eq. (2).

Specimens were tested to fracture in three-point bending at a crosshead displacement speed of 0.01 mm/s. The strain gage output was directly converted to strain reading by calibrating the strain gage output.

A test record consisting of an autographic plot of the output of the load sensing transducer vs the output of the strain gage was made for each specimen. The elastic modulus, E, was then calculated from the initial slope of the stress-strain curve.

The parameters varied in this investigation were polymer volume fraction, polymer particle size, and, qualitatively, the type of polymer and interfacial bonding between the ceramic and polymer phases. The polymer volume fraction was varied between 0.45 and 0.68. This selection provided elastic moduli somewhat higher than that of "dry bone."[31] To further lower the modulus of the composite, polymer volume fraction would have to be increased, which would result in very low strengths. This selection, therefore, can be viewed as a compromise between modulus and strength.[31]

Minimum pore size of the matrix is fixed due to limitations imposed by bone-tissue ingrowth. Hence, composites having mean pore sizes <100 μm were not investigated. On the other hand, the range of mean polymer particle size that can be fabricated is fixed when the polymer volume fraction is kept in the range of 0.45 to 0.68. This is seen clearly in Fig. 1. Hence, the range of polymer particle sizes that can be studied is fixed between approximately 380 and 680 μm. Fracture-surface micrographs of selected bend specimens were taken to determine the fracture mode and to study the fracture surfaces.

III. Results

The fracture-toughness and flexural-modulus and strength data are presented in Tables I to III and IV to VI, respectively. The improvement observed in critical strain energy release rate of PMMA-impregnated and coupled specimens was approximately four-fold over uncoupled specimens. PMMA, at a fixed polymer volume fraction and pore size, was 1.5 to 2 times more effective in increasing the fracture toughness of the ceramic than PBMA.

It is clear that a significant improvement has been achieved in flexural strength by incorporation of the polymer phase. The in-

crease in flexural strength of PMMA-impregnated and coupled samples was approximately three-fold over impregnated but uncoupled samples. The flexural strength increased at least four-fold and up to 18-fold over unfilled ceramic matrix. The increase in flexural strength of PBMA-filled and coupled samples was three- to eight-fold over unfilled samples. Therefore, coupled specimens were clearly superior to uncoupled specimens with respect to strength.

PMMA, at a fixed polymer volume fraction and particle size, increased the flexural strength of the ceramic 1.5 to 2 times more effectively than PBMA. This is due to the lower strength of PBMA, compared to PMMA, which reduces the stress-transfer effectiveness.

The effects of pore size and polymer volume fraction on flexural modulus are presented in Figs. 2 and 3, respectively. It is clear from Fig. 2 that flexural modulus is not a function of average particle size. Second-phase particle size does not appear as a variable in most models of elastic modulus for composites. However, shape and whether the second phase is dispersed or continuous normally influence the modulus. Since all particles in these composites were observed to be spherical, shape is not a concern in this study.

Figure 3 shows that the flexural moduli of the ceramic composites decrease with increasing polymer volume fraction. Also shown in Fig. 3 are a few data points obtained on porous ceramics which had no interconnected porosity. The solid line shows the data obtained by Coble and Kingery[32] from studies made on similar porous ceramics. It is evident that the flexural modulus is not improved by incorporation of a polymer phase.

Table IV. Flexural Modulus and Strength Data for PMMA-Impregnated Alumina Ceramic

Composite	Flexural modulus (GPa)	Flexural strength (MPa)
49.11C-PMMA650	72.3	65.0
51.99C-PMMA417	66.3	76.1
51.99C-PMMA417	55.2	76.5
52.00C-PMMA605	58.7	75.4
52.00C-PMMA605	66.5	82.7
52.00C-PMMA605	60.8	77.9
52.38C-PMMA585	59.1	69.3
52.38C-PMMA585	55.4	67.4
52.79U-PMMA410	70.0	21.4
52.79U-PMMA410	82.4	25.0
54.93C-PMMA520	47.6	63.3
55.26U-PMMA595	ND*	26.2
55.26U-PMMA595	43.7	24.0
55.26U-PMMA595	42.8	25.5
56.18C-PMMA471	51.7	78.4
56.18C-PMMA471	53.7	70.9
56.57C-PMMA608	43.5	57.0
56.57C-PMMA608	ND	58.3
57.90C-PMMA516	ND	65.2
57.90C-PMMA516	36.9	69.9
58.01C-PMMA605	41.3	57.5
58.19C-PMMA500	ND	61.8
58.19C-PMMA500	44.2	66.8
59.06C-PMMA525	31.5	74.3
59.06C-PMMA525	39.6	79.1
59.67U-PMMA431	37.5	26.8
59.67U-PMMA431	43.6	26.3
60.09C-PMMA473	37.9	60.1
60.09C-PMMA473	38.2	59.8
60.09C-PMMA473	44.8	60.1
61.81C-PMMA644	32.4	ND
61.81C-PMMA644	41.8	66.6
61.81C-PMMA644	41.7	64.2
63.20C-PMMA501	38.3	74.3
63.35C-PMMA482	38.2	81.7
63.40C-PMMA396	36.2	99.6
63.93C-PMMA404	40.9	95.2
63.93C-PMMA404	39.7	88.3
63.95C-PMMA384	36.0	68.8
65.07C-PMMA393	33.5	59.1
65.24U-PMMA395	29.4	18.4
65.24U-PMMA395	ND	18.8
67.03C-PMMA401	ND	109.0

*ND=not determined.

IV. Discussion

Linear elastic fracture mechanics is applicable only to brittle materials, where the amount of plastic deformation is small. Therefore, there will always be considerable uncertainty on the validity of the fracture-toughness data of PBMA composites. PBMA is rubbery in nature and, for a composite containing >50% PBMA, the extent of plastic deformation at the crack tip should be significant.

The critical strain energy release rate, G_c, was observed to be a function of both the polymer particle size and polymer volume fraction; G_c increased with increasing polymer volume fraction and decreasing polymer particle size. As the polymer volume fraction increases, more of the tougher phase is present in the composite, yielding a higher G_c value. Since larger particles are more-effective stress concentrators, it is reasonable to expect larger values of G_c

Table V. Flexural Modulus and Strength Data for PBMA-Impregnated Alumina Ceramic

Composite	Flexural modulus (GPa)	Flexural strength (MPa)
49.97C-PBMA576	78.3	42.9
49.97C-PBMA576	72.7	43.9
50.30C-PBMA453	73.8	39.4
50.30C-PBMA453	66.1	40.7
50.96C-PBMA483	54.8	42.4
50.96C-PBMA483	54.3	43.7
54.50C-PBMA574	47.3	36.8
54.50C-PBMA574	39.1	35.5
56.50C-PBMA494	36.4	45.3
56.50C-PBMA494	41.6	47.8
57.78C-PBMA573	43.7	39.7
57.78C-PBMA573	54.0	45.2
58.00U-PBMA368	47.6	18.7
58.00U-PBMA368	35.6	18.6
58.35C-PBMA527	45.7	41.0
58.35C-PBMA527	38.0	43.6
58.93C-PBMA569	40.9	39.1
60.28C-PBMA401	34.4	39.5
60.28C-PBMA401	36.9	38.8
60.79U-PBMA489	ND	10.0
60.79U-PBMA489	ND	10.9
63.97C-PBMA407	ND	41.1
64.93C-PBMA380	33.0	41.0
63.59U-PBMA457	34.9	11.6
63.59U-PBMA457	28.0	11.3

Table VI. Flexural Modulus and Strength Data for Unfilled Alumina Ceramic Matrix and Closed-Pore Alumina Ceramic

Sample*	Porosity (%)	Pore size (μm)	Flexural modulus (GPa)	Flexural strength (MPa)
CPC	21.6	ND	227.1	99.8
CPC	23.0	ND	215.4	91.1
CPC	23.4	ND	226.2	81.1
UCM	50.5	658	ND	14.2
UCM	51.9	658	ND	16.8
UCM	53.5	658	ND	13.8
UCM	58.5	610	ND	8.7
UCM	59.3	610	ND	7.2
UCM	59.5	610	ND	6.3
UCM	65.0	499	ND	7.6
UCM	65.8	499	ND	5.2
UCM	66.4	452	ND	4.0
UCM	66.6	452	ND	5.1

*UCM = unfilled alumina ceramic matrix; CPC = closed-pore alumina ceramic.

for composites having a smaller average particle size.

A nonlinear multiple regression[33–36] was run to fit different model equations to the data, as well as one linear multiple regression. The algorithm used is a modified version of the Marquardt program,[33] which is described in detail elsewhere.[30] The appropriate functional form to choose for G_c is not clear. Several forms were tried and the most favorable one, statistically, was chosen as the best fit:

$$G_c = (AF_p^a + B)/D^c \tag{5}$$

where A, B, a, and c are constants. Numerical values of these constants obtained from the nonlinear multiple regression give

$$G_c = (14.19F_p^{5.44} + 0.74)/D^{0.67} \tag{6}$$

where G_c is in J/m^2, and F_p and D are the polymer volume fraction and mean polymer particle size, respectively.

The critical stress intensity data obtained for coupled PMMA composites from CCT show a similar trend to that of G_c with respect to polymer volume fraction and polymer particle size. This trend, however, is somewhat disguised due to the decrease of modulus, E, with increasing polymer volume fraction. For coupled PBMA-impregnated composite specimens, K_{Ic}, however, decreases with increasing polymer volume fraction. For these composites, the decrease in modulus is more pronounced than the increase in G_c with increasing polymer volume fraction.

The critical stress intensity factor data obtained from the ASTM method seemed to be far less dependent on both the polymer volume fraction and polymer particle size for coupled, PMMA-impregnated composites. Figure 4 shows the ASTM fracture toughness data vs CCT fracture-toughness data. Ideally, one would expect the data points to fall on the 45° line if both methods measured the fracture toughness equally. It is clear from the plot that data points measured using the ASTM method are lower than the data points measured using the CCT. The ASTM method was developed primarily for metals and some of the empirical criteria may not be the best choice for ceramics and polymers. It is still being argued whether the ASTM method is overly conservative in estimating fracture toughness even for metals.[37] In fact, many researchers measuring the fracture toughness of ceramics and polymers have relaxed these criteria. Some, for instance, use P_{max} in Eq. (3) instead of P_Q.[38–41] Since P_{max} is always higher than P_Q, the K_{Ic} calculated will be larger, and equal to K_{Ic} values measured by using the CCT.

The authors believe that the CCT, although more tedious, is more liberal in that it imposes fewer restrictions on the testing procedure. When both methods measure equal values for K_{Ic}, however, use of the ASTM method can save time. Since the ASTM method is faster and easier to apply, the authors recommend its use, with P_{max} replacing P_Q in the published procedure. In the analysis following these pages, however, only the data obtained from the CCT for PMMA will be used.

Finally, the fracture mode observed in the composite material depended on whether the sample was coupled or not. Figure 5(*A*)

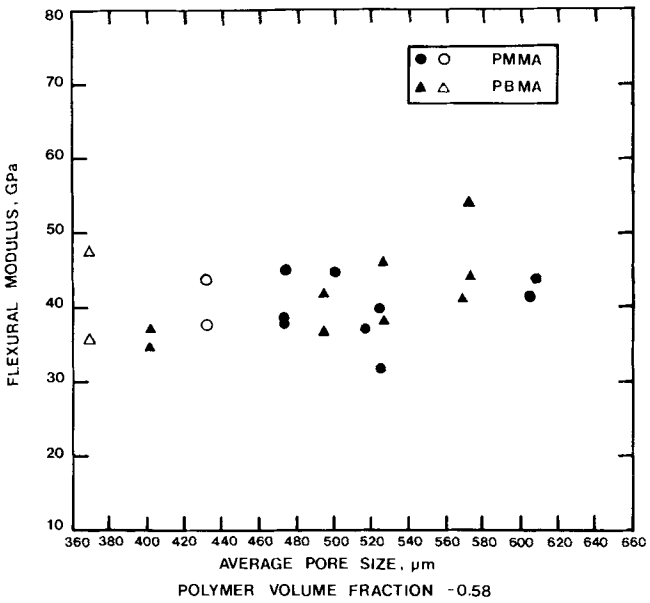

Fig. 2. Flexural modulus of poly(methyl methacrylate)- and poly(butyl methacrylate)-impregnated ceramics as a function of average pore size (●, ▲ and ○, △ represent coupled and uncoupled composites, respectively).

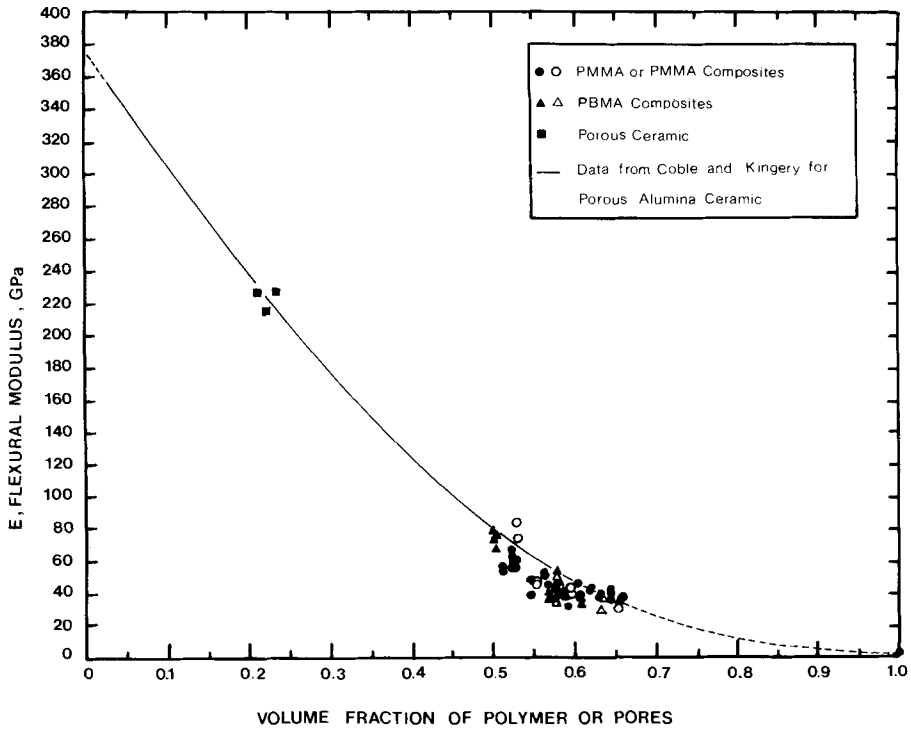

Fig. 3. Flexural modulus of poly(methyl methacrylate)- and poly(butyl methacrylate)-impregnated ceramics as a function of polymer volume fraction (●, ▲ and ○, △ represent coupled and uncoupled composites, respectively, and ■ represents porous ceramic).

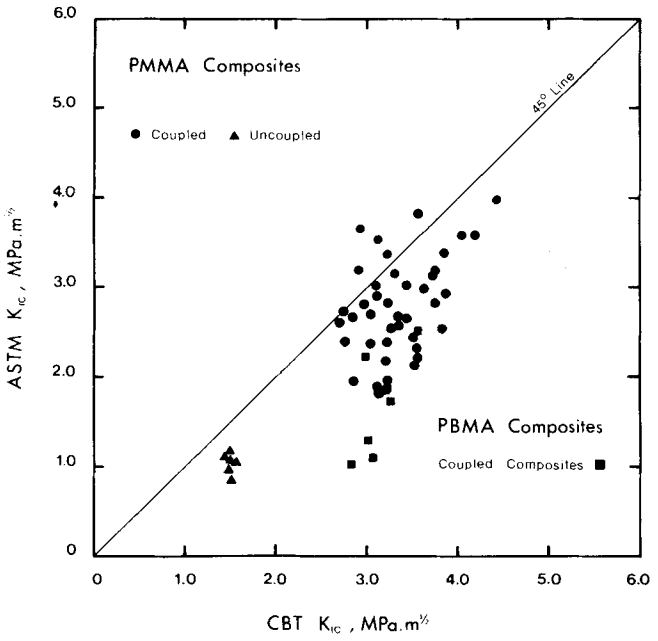

Fig. 4. Comparison of critical stress intensity factors measured by different methods.

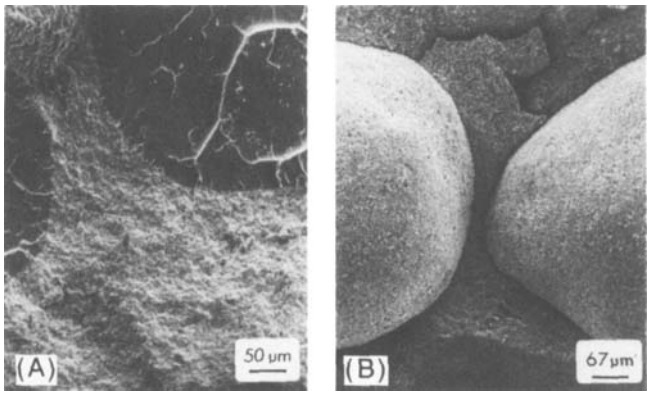

Fig. 5. Fracture surfaces of (*A*) coupled and (*B*) uncoupled poly(methyl methacrylate)/alumina composites, showing fracture paths through and around polymer particles, respectively.

shows a fracture surface for a PMMA-alumina composite where the two phases are coupled using the silane coupling agent. The fracture path in this micrograph is transparticle, passing through both the ceramic and polymer phases. Figure 5(*B*) shows the fracture surface of an uncoupled PMMA-alumina composite. Here, the fracture path passes around the polymer particles, which are thus prevented from absorbing energy during crack propagation. This important result also accounts for the higher strength and fracture surface energy of coupled specimens compared with uncoupled specimens. A crack propagating through the brittle ceramic phase and tougher polymer phase obviously requires more energy than a crack propagating only in the ceramic phase.

Higher strengths measured for coupled specimens can also be explained by following a similar argument, i.e., a coupled interface can transfer stress, whereas an uncoupled interface cannot. Thus, when coupled, the polymer phase behaves more like a part of the continuum and is less likely to cause severe stress intensification. There will be some stress intensification, however, due to moduli mismatch of the two phases. On the other hand, some small stress transfer is still possible in the uncoupled specimens due to the three-dimensional skeletal structure of the incorporated polymer phase. This is the main reason for the difference between the strengths of filled but uncoupled specimens and unfilled ceramic at a given porosity.

For PMMA-impregnated specimens, the flexural strength decreases with increasing average particle size and polymer volume fraction. Since the ceramic is the stronger component, it is reasonable to expect the strength to decrease with increasing polymer volume fraction. It is also known that larger particles are more effective stress concentrators,[42] causing failure at smaller loads. For PBMA-impregnated specimens, the flexural strength seems to be independent of polymer volume fraction or particle size. This rather unexpected behavior can be explained only after the moduli data are discussed in the following paragraphs.

Figure 3 shows that the data points obtained for the composite material fall very close to the experimental modulus line drawn for unfilled porous alumina ceramics. It appears that the load is mostly carried by the ceramic phase. This seems reasonable if one considers the moduli ratio of the ceramic and polymer phases. In the case of PMMA-impregnated specimens, the ratio of flexural modulus of the ceramic phase to that of the polymer phase is more than 150; for PBMA-impregnated specimens this ratio is more than 900. Thus, the flexural modulus of the composite is very close to that of a ceramic having a porosity equal to the polymer volume fraction of that composite. Another evidence of all load being carried by the ceramic phase can be seen in the case of uncoupled specimens. Although there was almost no stress transfer between the phases, the flexural moduli of the uncoupled composites were equal to those of coupled samples.

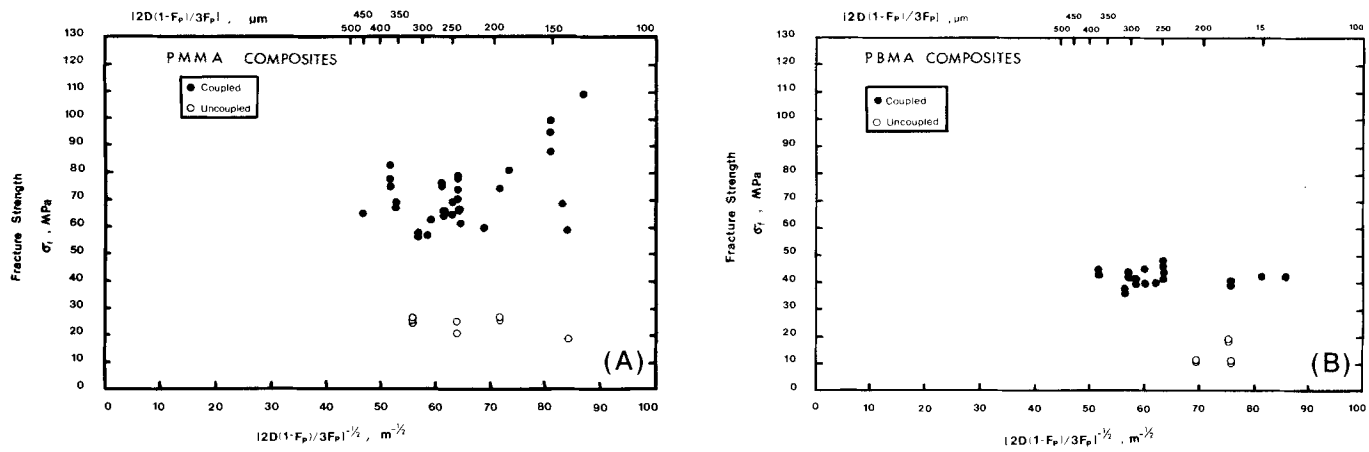

Fig. 6. Fracture strength vs inverse on square root of interparticle spacing for (*A*) poly(methyl methacrylate)- and (*B*) poly(butyl methacrylate)-impregnated composites.

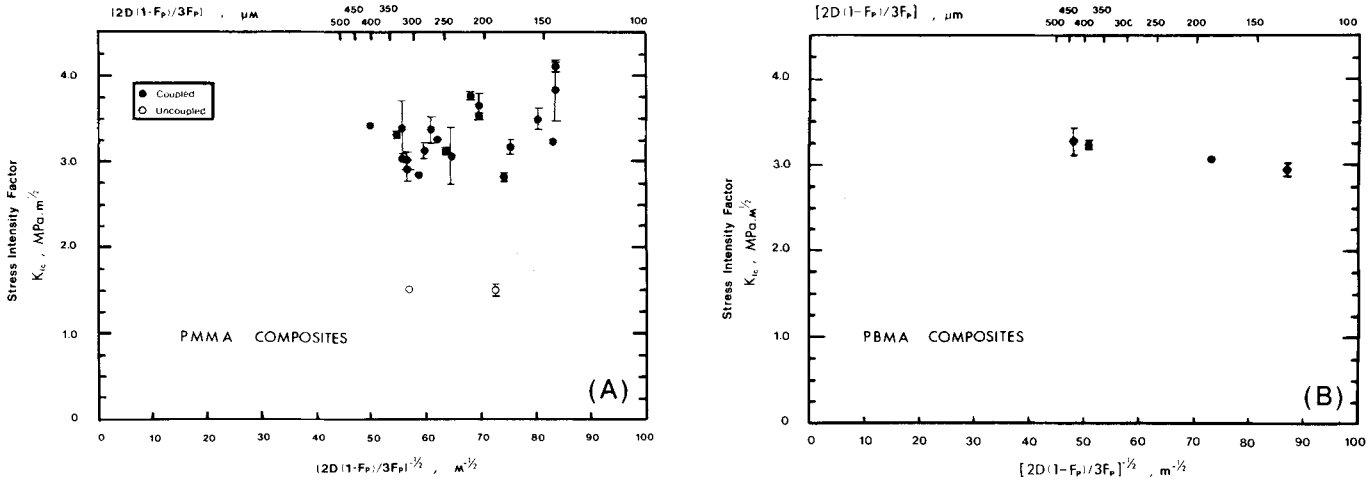

Fig. 7. Critical stress intensity factor vs inverse square root of interparticle spacing for (*A*) poly(methyl methacrylate)- and (*B*) poly(butyl methacrylate)-impregnated composites.

The effect of porosity, P, on elastic modulus has been represented by several equations.[43–45] The best known and statistically the most favorable one is[44]

$$E = E_0 \exp(-kP) \tag{7}$$

where k is a constant and E_0 is the modulus at zero porosity. The linear regression fit to the experimental data obtained in this study and eight data points for zero-porosity alumina ceramic taken from the literature[32,46–48] yielded

$$E = 439.75 \exp(-3.96P) \tag{8}$$

where E is the composite elastic modulus in GPa.

Fullman[49] reported relations that can be used to compute the spacing d between spheres of uniform size D embedded within a matrix material

$$d = 2D(1 - F_s)/3F_s \tag{9}$$

where F_s is the volume fraction of the spheres. Replacing F_s by F_p in this equation, an interparticle spacing between the polymer particles can be obtained. It will be shown later that this spacing is very critical for this composite material as it is approximately equal to the length of the interparticle cracks that are believed to cause the composite to fail. Figure 6 shows the fracture strength as a function of the inverse square root of interparticle spacing for PMMA- and PBMA-impregnated composites. The strength of coupled PMMA composites increases as the interparticle spacing decreases. The strength of uncoupled composites and PBMA-impregnated ceramic, however, is independent of the interparticle spacing. Figure 7 helps to explain why this is so, together with the following general form of the strength equation

$$\sigma_f \propto K_{Ic} \cdot (1/d^{1/2}) \tag{10}$$

In Fig. 7(*A*), the stress intensity factor of PMMA composites increases with increasing inverse square root of interparticle spacing. Both this conclusion and the strength increase with $1/d^{1/2}$ have resulted from a statistical analysis of the data. Thus, the product in Eq. (10) will increase. This means that strength should increase with increasing $1/d^{1/2}$. In other words, strength increases with decreasing interparticle spacing (or decreasing flaw size). This is what has been observed in Fig. 6(*A*). Figure 7(*B*), on the other hand, shows a decrease of K_{Ic} for PBMA composites with increasing $1/d^{1/2}$. A decrease in K_{Ic} in Eq. (10) is therefore cancelled by an increase in $1/d^{1/2}$, yielding an almost constant strength when plotted as a function of $1/d^{1/2}$. Figure 7(*B*) also shows that coupling increases the fracture toughness of PMMA composites by at least two fold.

In 1956, Bowie[50] proposed a solution of the class of plane problems corresponding to a distribution of radial cracks emanating from the boundary surface of a circular hole in an infinite plate under uniaxial and biaxial loading conditions. He arrived at the following expression

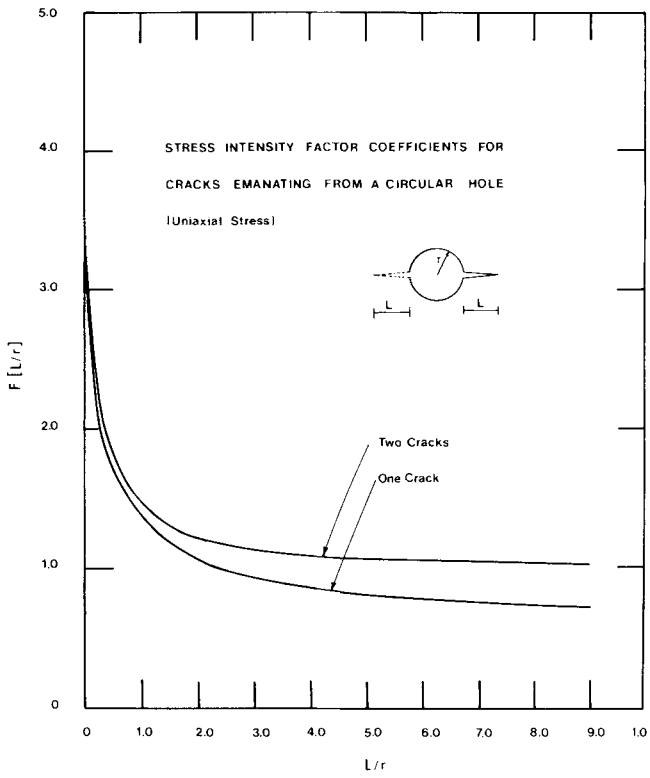

Fig. 8. Stress intensity factor coefficients for single- and double-crack versions of Bowie model for uniaxial loading conditions.

$$K_I = \sigma(L\pi)^{1/2}F(L/r) \tag{11}$$

where L is the length of the crack, r the radius of the hole, and F the stress intensity factor coefficient which is a function of the ratio L/r. Figure 8 shows this coefficient for the single- and double-crack versions of the Bowie model for the uniaxial loading condition.

Consider now the contribution of the polymer particles to the fracture resistance. Many micrographs taken during the SEM study of the fracture surfaces indicated the presence of single, double, and multiple cracks running from one polymer particle to a neigh-

boring polymer particle. Figure 9 shows the case where two cracks are emanating from a polymer particle. These cracks were most probably formed during fabrication of the composite specimens.

In order to apply the Bowie model to the composite material studied in this investigation, the cracks must be shown to be present in the samples before they are stressed. In other words, it must be demonstrated that these cracks were not formed during stressing of the test specimens. This can be checked by examining the orientation of the cracks. If the cracks were formed during testing, they should have a preferred orientation with respect to the direction of the applied stress or crack extension. A random orientation, however, will rule out such a possibility; SEM micrographs show that cracks do not have any particular orientation and support the argument that they were formed during the fabrication process.[30]

If Eqs. (5), (7), and (9) are now introduced into Eq. (11), a fracture strength equation based on the Bowie model is obtained

$$\sigma_f = 1/F(L/r)\,[(3E_0 \exp(-kF_p)\,(AF_p^a + B))/(2\pi D^{1+C}(1 - F_p))]^{1/2} \quad (12)$$

This equation predicts that strength is only a function of F_p and D, which are relatively easy to measure. A, B, E_0, k, a, and c are constants, values of which have already been determined through regression analysis. Introducing these

$$\sigma_f = 1/F(L/r)\,[2.1 \times 10^{11} \exp(-3.96F_p)\,(14.19F_p^{5.44} + 0.74) \times F_p/(D^{1.67}(1 - F_p))]^{1/2} \quad (13)$$

where σ_f is the predicted fracture strength in Pa. Figure 10 shows the predicted strengths vs measured strengths for single-crack and double-crack versions of the Bowie model. Although predictions by the double-crack version are better, both versions predict slightly higher strengths than measured. It is important to recognize that both versions use the straight distance between the polymer particles as the critical flaw size. In reality, the crack path is never straight and it is almost impossible to determine the true length of the critical flaw; SEM micrographs show varying degrees of crack-path tortuosity. Since location of the flaw that causes failure is extremely difficult, the fracture of any particular sample could have been controlled by single- , double- , or multiple-crack mechanisms. In any case, if one takes into account a 10 to 30% variation in crack-path tortuosity for both versions of the model, the predicted strengths move closer to the 45° line. Figure 11 illustrates how the predicted strengths change with a 30% crack-path tortuosity allowance for single- and double-crack versions of the model. Here, again, scatter in the data could be explained on the basis that different mechanisms might be controlling different samples. It is possible that those samples with high predicted strengths have either longer crack-path tortuosity or multiple cracks (or double crack instead of single, or vice versa) as the critical flaws that caused fracture.

Defects present in the samples also contribute to the scatter in the data. Occasionally, a few unfilled pores, interface cracks, or inhomogeneities have been observed. Closed unfilled pores were not detected at any time during the fractographic studies, but their presence cannot be ruled out.

In conclusion, the Bowie model is useful in describing strengths of these composites. Furthermore, the Bowie model provides considerable insight on the possible mechanisms controlling the fracture of the polymer-ceramic composite.

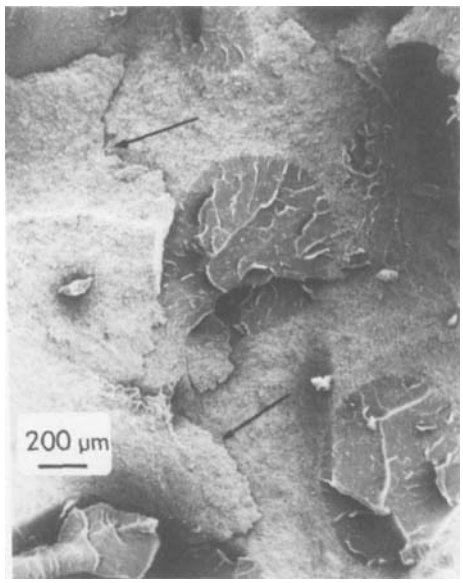

Fig. 9. Double crack through ceramic phase in poly(methyl methacrylate)/alumina composite.

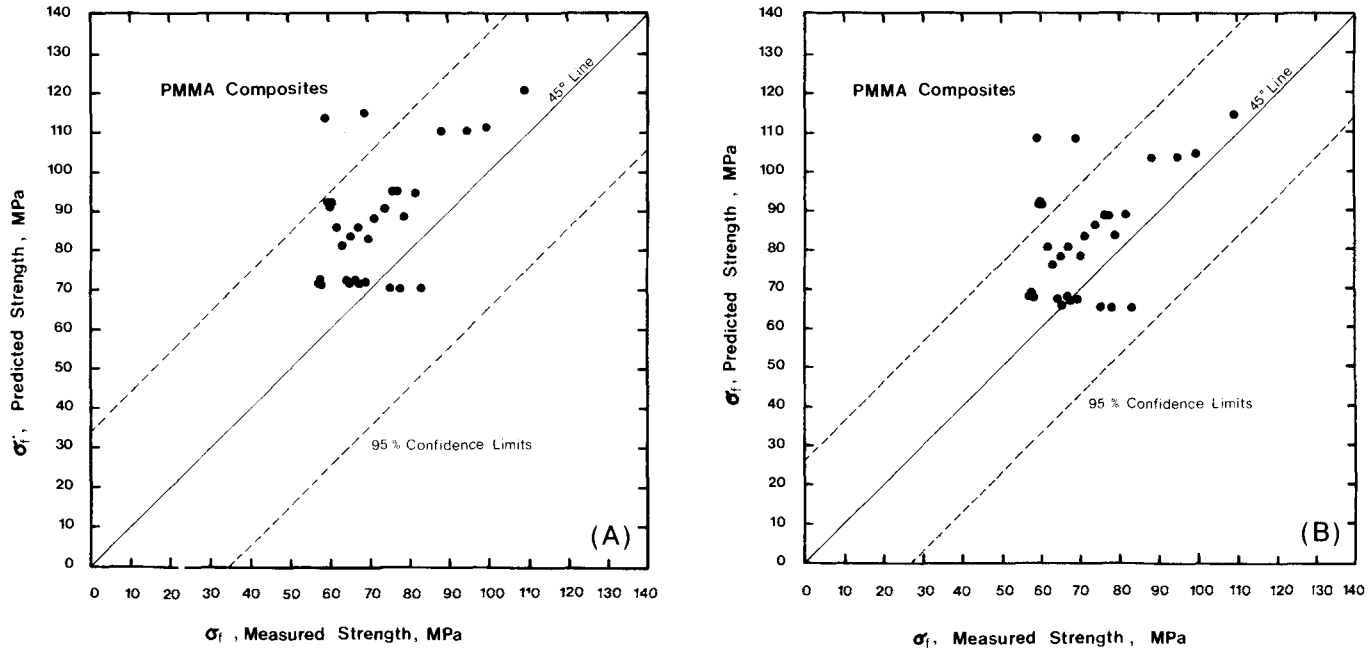

Fig. 10. Predicted fracture strength vs measured fracture strength for (*A*) single-crack version and (*B*) double-crack version of Bowie model.

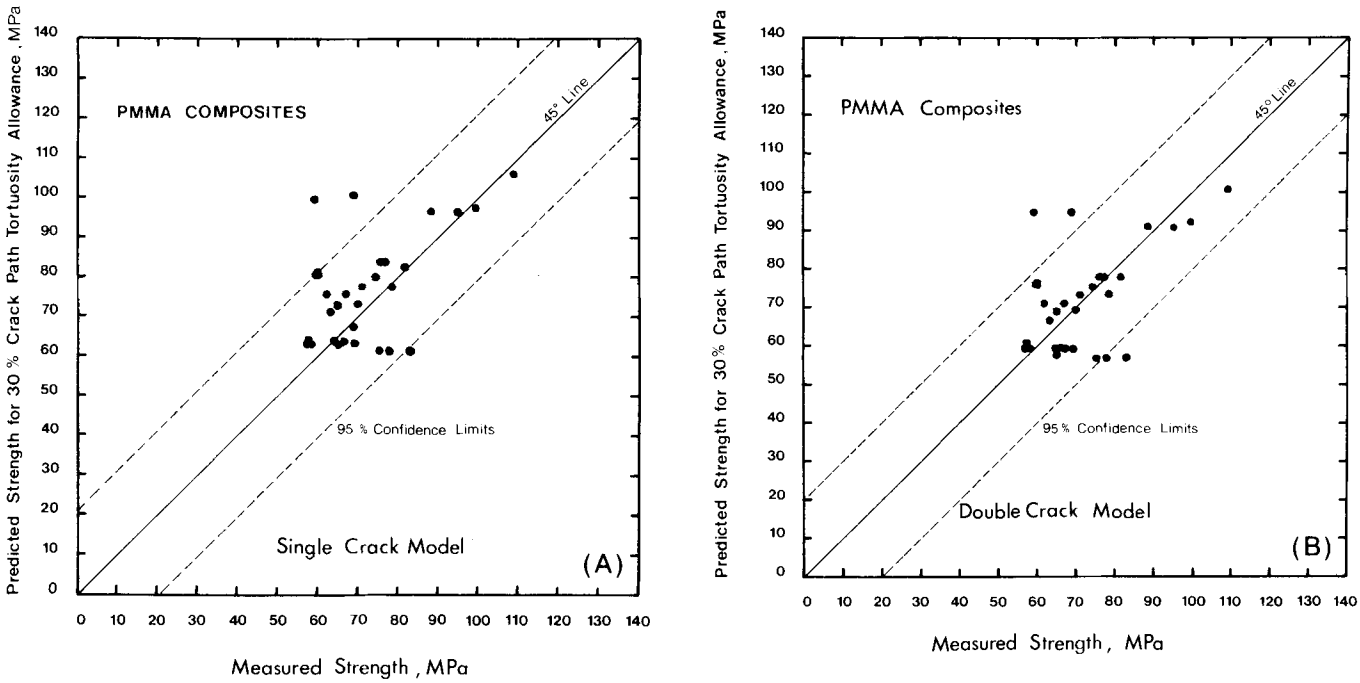

Fig. 11. Predicted fracture strength for 30% crack-path tortuosity allowance vs measured fracture strength for (*A*) single- and (*B*) double-crack versions of Bowie model.

References

[1]B. W. Sauer, A. M. Weinstein, J. J. Klawitter, S. F. Hulbert, R. B. Leonard, and J. G. Bagwell, "The Role of Porous Polymeric Materials in Prosthesis Attachment," *J. Biomed. Mater. Res. Symp.*, **8** [5] 145–53 (1974).

[2]C. D. Talbert, "A Basic Investigation Into The Potential of Ceramic Materials as Permanently Implantable Skeletal Prosthesis"; M.Sc. Thesis, Clemson University, Clemson, SC, 1969.

[3]A. M. Struthers, "Experimental Study of Polyvinyl Sponge as Substitute for Bone," *Plastic Reconstr. Surg.*, **15**, 274–79 (1955).

[4]E. P. Henefer, T. A. McFall, and D. C. Hauschild, "Acrylamide Sponge for Repair of Alveolar Bone Defects," *J. Oral Surg.*, **26**, 577–81 (1968).

[5]L. Smith, "Ceramic-Plastic Materials as a Bone Substitute," *Arch. Surg.*, **87**, 653–59 (1963).

[6]J. S. Hirschhorn and J. T. Reynolds, "Powder Metallurgy Fabrication of Cobalt Alloy Surgical Implant Materials," The University of Wisconsin, 1975; p. 137.

[7]J. Gebauer, D. P. H. Hasselman, and R. E. Long, "Effect of Polymer Impregnation on Physical and Mechanical Behavior of Ceramic Tile Bodies," *Am. Ceram. Soc. Bull.*, **51** [5] 471–73 (1972).

[8]A. Auskern and W. Horn, "Some Properties of Polymer Impregnated Cements and Concretes," *J. Am. Ceram. Soc.*, **54** [6] 282–85 (1971).

[9]M. Steinberg, L. E. Kukacha, P. Colombo, and B. Manowitz, "Preparation and Characteristics of Concrete-Polymer Composites"; pp. 547–61 in Multicomponent Polymer Systems (Advances in Chemistry Series, No. 90). Edited by R. F. Gould. The American Chemical Society, Washington, DC, 1971.

[10]D. G. Manning and B. B. Hope, "The Effect of Porosity on The Compressive Strength and Elastic Modulus of Polymer Impregnated Concrete," *Cem. Concr. Res.*, **1**, 631–35 (1971).

[11]J. R. Clifton, J. E. Fearn, and E. D. Anderson, "Polymer Impregnated Hardened Cement Pastes and Mortars," *Natl. Bur. Stand., Build. Sci. Ser.*, **83**, 21–25 (1976).

[12]D. P. H. Hasselman, J. Gebauer, and J. A. Manson, "Elastic Behavior of Polymer-Impregnated Porous Ceramics," *J. Am. Ceram. Soc.*, **55** [12] 588–91 (1972).

[13]P. R. Hills, R. L. Barrett, and R. J. Pateman, "The Radiation Polymerization of Impregnated Fibrous Materials," U.K. Atomic Energy Agency, Rept. AERE–R–6090, 1969.

[14]J. E. Langwig, J. A. Meyer, and R. W. Davidson, "Influence of Polymer Impregnation on Mechanical Properties of Basswood," *For. Prod. J.*, **18** [17] 33–36 (1968).

[15]J. E. Langwig, J. A. Meyer, and R. W. Davidson, "New Monomers Used in Making Wood-Plastics," *For. Prod. J.*, **19** [11] 57–61 (1969).

[16]J. F. Siau, R. W. Davidson, J. A. Meyer, and C. Shaar, "A Geometrical Model for Wood-Polymer Composites," *Wood Sci.*, **1** [12] 116–28 (1968).

[17]J. J. Klawitter, B. W. Sauer, A. M. Weinstein, and S. F. Hulbert, "Characterization of Tissue Growth into Porous Biomaterials," Tech. Rept. No. 7; submitted to Office of Naval Research, 1974.

[18]"Standard Method of Test for True Specific Gravity of Refractory Material by Water Immersion," *ASTM Stand.*, C135–66, Part 13, 1973.

[19]W. D. Kingery, Introduction to Ceramics. Wiley & Sons, New York, 1967; pp. 412–17.

[20]S. F. Hulbert, J. J. Klawitter, B. W. Sauer, and J. R. Matthews, "Characterization of Tissue Ingrowth into Porous Bioceramics," Tech. Rept. No. 2; submitted to Office of Naval Research, 1972.

[21]R. W. Treharne and N. Brown, "Factors Influencing the Creep Behavior of Poly(methyl methacrylate) Cements," *J. Biomed. Mater. Res.*, **9** [4] 81–88 (1975).

[22]D. C. Smith, "The Acrylic Denture Base: Mechanical Evaluation of Dental Poly(-methyl methacrylate)," *Br. Dental J.*, **111** [1] 9–14 (1961).

[23]W. L. Jaffe, R. M. Rose, and E. L. Radin, "On The Stability of The Mechanical Properties of Self-Curing Acrylic Bone Cement," *J. Bone Joint Surg.*, **56-A** [8] 1711–14 (1974).

[24]S. S. Haas, G. Dickson, and G. M. Brauer, "A Proposed Specification for Acrylic Bone Cement," *J. Biomed. Mater. Res.*, **9** [4] 105–17 (1975).

[25]D. M. Fisher, R. T. Bubsey, and J. E. Srawley, "Design and Use of a Displacement Gauge for Crack Extension Measurements," NASA TN–D–3724, NASNA, National Aeronautics and Space Administration, 1966.

[26]W. F. Brown, Jr. and J. E. Srawley, "Plane-Strain Crack Toughness Testing of High Strength Metallic Materials," STP 410, American Society for Testing and Materials, Philadelphia, 1966.

[27]A. G. Evans; pp. 17–29 in Fracture Mechanics of Ceramics, Vol I. Edited by R. C. Bradt, D. P. H. Hasselman, and F. F. Lange. Plenum, New York, 1974.

[28]G. R. Irwin and J. A. Kies, "Critical Energy Rate Analysis of Fracture Strength," *Weld. J. Res. Suppl.*, **33**, 193–98 (1954).

[29]"Standard Method of Test for Plane-Strain Fracture Toughness of Metallic Materials," *ASTM Stand.*, E399–74, Part 10, 1974.

[30]S. Yalvaç, "Fracture Behavior of Ceramic-Polymer Composite Biomaterials"; Ph.D. Thesis, The University of Michigan, 1982; pp. 179–95.

[31]G. Hermann and H. Liebowitz; pp. 771–836 in Fracture, Vol. 7. Edited by H. Liebowitz. Academic Press, New York, 1972.

[32]R. L. Coble and W. D. Kingery, "Effect of Porosity on Physical Properties of Sintered Alumina," *J. Am. Ceram. Soc.*, **39** [11] 377–85 (1956).

[33]D. W. Marquardt, "Least Squares Estimation of Nonlinear Parameters, A Computer Program in Fortran IV Language," IBM Share Library, Distribution Number 3094, 1964.

[34]J. L. Kuester and J. H. Mize; pp. 240–53 in Optimization Techniques With Fortran. McGraw-Hill, New York, 1973.

[35]P. R. Bevington; pp. 233–39 in Data Reduction and Error Analysis For The Physical Sciences. McGraw-Hill, New York, 1969.

[36]E. Gulari and B. Bedwell; private communications.

[37]J. G. Kaufman in Developments in Fracture Mechanics Test Methods Standardization. Edited by W. F. Brown and J. G. Kaufmann. STP 632, American Society for Testing and Materials, 1977.

[38]L. A. Simpson, T. R. Hsu, and G. Merrett, "The Application of The Single-Edge Notched Beam to Fracture Toughness Testing of Ceramics," *J. Test. Eval.*, **2** [6] 503–509 (1974).

[39]T. R. Guess and W. R. Hoover, "Fracture Toughness of Carbon-Carbon Composites," *J. Comp. Mater.*, **7**, 2–20 (1973).

[40]D. G. Smith and M. Chowdary, "The Fracture Toughness of Slip-Cast Fused Silica," *Mater. Sci. Eng.*, **20**, 83–88 (1975).

[41]G. G. Chell, "An Assessment of Some Methods of Obtaining Fracture Toughness Values From Invalid Test Data," *Mater. Sci. Eng.*, **24**, 233–38 (1976).

[42]F. F. Lange; pp. 22–68 in Composite Materials, Vol. 5. Edited by L. J. Broutman. Academic Press, New York, 1974.

[43]R. W. Davidge and A. G. Evans, "The Strength of Ceramics," *Mater. Sci. Eng.*, **6**, 281–98 (1970).

[44]R. M. Spriggs, "Expression for Effect of Porosity on Elastic Modulus of Polycrystalline Refractory Materials, Particularly Aluminum Oxide," *J. Am. Ceram. Soc.*, **44** [12] 628–29 (1961).

[45]J. K. McKenzie, "Elastic Constants of a Solid Containing Spherical Holes," *Proc. Phys. Soc. (London)*, **63B**, 2–11 (1950).

[46]W. B. Crandall, D. H. Chung, and T. J. Grany; paper presented at Conference on Mechanical Properties of Engineering Ceramics, North Carolina State College, Raleigh, 1960.

[47]R. M. Spriggs and T. Vasilos, "Effect of Grain Size and Porosity on the Transverse Bend Strength and Elastic Modulus of Hot Pressed Alumina and Magnesia"; for abstract see *Am. Ceram. Soc. Bull.*, **40** [4] 187 (1961).

[48]S. M. Lang, "Properties of High-Temperature Ceramics and Cermets, Elasticity and Density at Room Temperature," *Natl. Bur. Stand. Monograph*, **6**, 1–45 (1960).

[49]R. L. Fullman, "Measurement of Particle Sizes in Opaque Bodies," *Trans. AIME*, **197**, 447–52 (1953).

[50]O. L. Bowie, "Analysis of An Infinite Plate Containing Radial Cracks Originating at The Boundary of An Internal Circular Hole," *J. Math. Phys.*, **35**, 60–71 (1956).